Persistent Low Overcast Events in the U.S. Upper Midwest: A Climatological and Case Study Analysis

PAUL J. ROEBBER, JAMES M. FREDERICK, AND THOMAS P. DEFELICE

Department of Geosciences, University of Wisconsin—Milwaukee, Milwaukee, Wisconsin

(Manuscript received 24 August 1997, in final form 31 March 1998)

ABSTRACT

Persistent low overcast conditions, defined as continuous overcast conditions (100% cloud cover) with ceiling heights at or below 2 km for a minimum of 5 days, are found to occur in the cold season in the U.S. upper Midwest on average slightly more often than once every two years. These occurrences are associated with two primary large-scale circulation patterns. Most commonly, the midlatitude westerlies are split across North America, with downstream confluence of the northwesterly polar and the southwesterly subtropical jet streams. A second, less frequent, pattern features an amplified westerly jet across North America, with a correspondingly rapid progression of weakly developed cyclones through the region. In the case of the split flow pattern, composite surface high pressure is established, occasionally disrupted by the emergence from either stream of relatively weak cyclones. These systems act to moisten the affected region at low levels through horizontal transport of moisture and, to a lesser extent, moisture convergence. Subsidence inversions established following the passage of these systems act to slowly erode the depth of the surface-based moist layer but are insufficient in combination with the weak solar radiative input to dissipate the cloud. The properties of the event structure, from the large scale down to that of the cloud layer itself, are stable. Under such conditions, the mechanism that finally removes the cloud is the passage of a relatively well-developed baroclinic wave and its associated forcing (subsidence, dry air advection, moisture divergence). Correspondingly, the difficult act of forecasting the end of such periods requires an accurate assessment of the sufficiency of that forcing to remove the low-level cloud. It is suggested that a relatively simple one-dimensional boundary layer model employed for the time to be critically tested in conjunction with the standard forecast model guidance (forecast vertical motion, profiles of temperature and moisture, Model Output Statistics cloud cover and ceiling) would provide additional information regarding forecast uncertainty.

1. Introduction

National Weather Service (NWS) operations support commercial and general aviation through their forecast services; accordingly, the forecasting of the onset and duration of low cloud ceilings is potentially of considerable economic value and directly impacts public safety. Low overcast conditions, because of their impact on the radiative balance of the earth–atmosphere system, may also have significant climatic effects (Twomey 1991). In addition, persistent low overcast events (PLOEs) likely contribute to the winter malaise that accompanies life in northern latitudes (Morgan and Moran 1997, 79–90). Unfortunately, the onset and breakup of low overcast conditions are often difficult to predict. As an example, we show in Table 1 the observed and Model Output Statistics (MOS) best category forecast for cloud amount for a particularly long overcast event at Milwaukee, Wisconsin (see section 3 for a detailed analysis of this case). Although the MOS 6-h forecasts appear to capture the observed cloud cover quite well, there is a marked tendency for the forecasts to reduce the cloud cover as the integrations proceed (which can be seen by following the forecasts along a diagonal in Table 1). As a consequence, forecast skill [where the forecasts are composed of the MOS cloud category probability forecasts and skill is measured by the ranked probability score using the 1961–90 December–January climatology as a baseline; see Epstein (1969) for details concerning this verification measure] falls rapidly from 0.467 at 6-h range to −0.172 by 18 h (−0.210 and −0.201 at 30 h and 42 h, respectively). Thus, higher forecast skill was attainable through the use of climatology (22% CLR, 12% SCT, 12% BKN, and 54% OVC) at all but the shortest forecast range for this event. In the concluding discussion, we will reference a very recent example of a PLOE that demonstrates that these events represent a continuing forecast challenge. We are thus motivated to understand the inherent physical processes that control these events. With this understanding, a means to provide better predictions

Corresponding author address: Dr. Paul J. Roebber, Department of Geosciences, University of Wisconsin—Milwaukee, Lapham Hall 352, P.O. Box 413, Milwaukee, WI 53201.
E-mail: roebber@csd.uwm.edu

© 1998 American Meteorological Society

Unauthenticated | Downloaded 05/10/21 09:57 PM UTC

TABLE 1. Observed and NGM-MOS best category forecast for cloud amount (CLR = clear skies, SCT = scattered, BKN = broken, and OVC = overcast) for different forecast ranges at Milwaukee, WI (MKE), for the PLOE of 26 December 1991–10 January 1992. The date is shown in YYMMDDHH format. Boldface MOS cloud categories indicate that the forecast was correct.

Date	OBS	06 h	18 h	30 h	42 h
91122618	OVC	SCT	BKN	SCT	SCT
91122706	OVC	**OVC**	BKN	SCT	CLR
91122718	OVC	**OVC**	CLR	CLR	CLR
91122806	OVC	**OVC**	CLR	CLR	CLR
91122818	OVC	**OVC**	**OVC**	**OVC**	SCT
91122906	OVC	**OVC**	**OVC**	**OVC**	**OVC**
91122918	OVC	**OVC**	BKN	**OVC**	**OVC**
91123006	OVC	**OVC**	SCT	SCT	BKN
91123018	OVC	**OVC**	SCT	SCT	SCT
91123106	OVC	**OVC**	**OVC**	CLR	CLR
91123118	OVC	**OVC**	**OVC**	**OVC**	BKN
92010106	OVC	**OVC**	BKN	**OVC**	**OVC**
92010118	OVC	**OVC**	**OVC**	**OVC**	**OVC**
92010206	OVC	**OVC**	**OVC**	**OVC**	**OVC**
92010218	OVC	**OVC**	**OVC**	**OVC**	**OVC**
92010306	OVC	**OVC**	**OVC**	**OVC**	**OVC**
92010318	OVC	**OVC**	**OVC**	**OVC**	**OVC**
92010406	OVC	**OVC**	**OVC**	**OVC**	**OVC**
92010418	OVC	CLR	CLR	CLR	BKN
92010506	OVC	**OVC**	CLR	CLR	CLR
92010518	OVC	**OVC**	BKN	SCT	BKN
92010606	OVC	**OVC**	**OVC**	**OVC**	**OVC**
92010618	OVC	**OVC**	BKN	SCT	SCT
92010706	OVC	**OVC**	SCT	CLR	CLR
92010718	OVC	**OVC**	**OVC**	**OVC**	SCT
92010806	OVC	**OVC**	**OVC**	**OVC**	**OVC**
92010818	OVC	**OVC**	**OVC**	**OVC**	**OVC**
92010906	OVC	**OVC**	**OVC**	**OVC**	**OVC**
92010918	OVC	**OVC**	**OVC**	**OVC**	**OVC**
92011006	OVC	**OVC**	SCT	**OVC**	**OVC**
92011018	SCT	OVC	**SCT**	**SCT**	**SCT**

may be developed that could mitigate their adverse effects.

This paper will focus on the development and evolution of PLOEs in the upper midwestern United States. In this context, a low overcast is taken to be cloud coverage of 100% with a base below 2000 m, consistent with the World Meteorological Organization (WMO) definition of stratiform cloud (WMO 1975). PLOEs will be considered to be those low cloud conditions as defined above whose continuous duration exceeds the timescale of synoptic-scale weather events (taken to be 5 days). Our focus on persistent events is a tacit recognition that there is no information on the climatological and synoptic characteristics of such periods. Shorter duration events, which occur at higher frequency (see section 2a), are certainly of operational concern but are easily treatable within the framework of short-range forecasting (e.g., Shea 1996). In section 2, a climatological analysis of the duration and seasonality of PLOEs along with their synoptic and large-scale signatures will be provided. In section 3, a detailed case study of the 1991–92 event will be presented. The case study will include analyses of the evolution of the atmospheric profiles of temperature and moisture as obtained from surface and rawinsonde observations and from experiments with a one-dimensional planetary boundary layer (PBL) model. Finally, a concluding discussion with recommendations for forecasters will be presented in section 4.

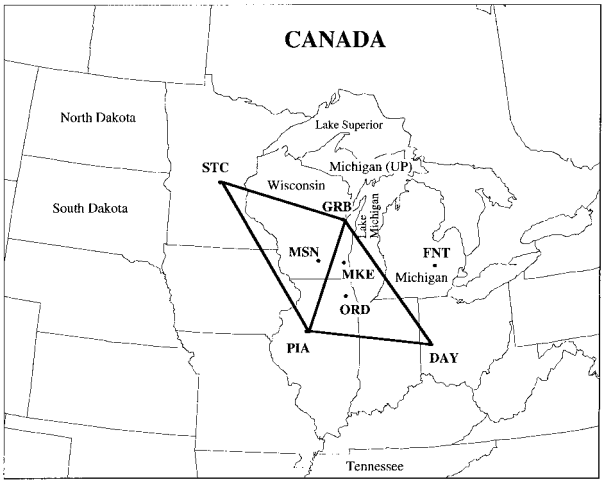

FIG. 1. A locator map for place names discussed in the text. Also shown are the orientations of the two triangles (STC–PIA–GRB and PIA–DAY–GRB) used to compute dynamical quantities and the moisture budget terms. See text for details.

2. Climatology of low overcast conditions

In this section, we seek to provide a climatological context for interpreting the analysis of the specific PLOE to be presented in section 3. In particular, we wish to examine the historical record of PLOEs to establish length and seasonality (section 2a), to identify characteristic lower-tropospheric signatures associated with PLOEs (section 2b), and to quantify those signatures through the application of the concept of regional analogs (section 2c; see Roebber and Bosart 1998).

a. Historical record of PLOEs

The climatological behavior of PLOEs was examined at two cities in southern Wisconsin (Madison, MSN; and Milwaukee, MKE; see Fig. 1) using 30 yr (1961–90) of surface observations obtained from the Solar and Meteorological Surface Observation Network CD-ROM prepared by the National Climatic Data Center. The analysis (Fig. 2) shows that low overcast conditions are a common occurrence in southern Wisconsin, particularly in the cold season (November–April). These results are consistent with similar analyses performed in other regions of the United States (Shea 1996). However, the majority of the events continue for 48 h or less (Fig. 3). PLOEs, that is those episodes lasting for at least 120 h, occurred on 14 (12) occasions in the 30 yr of record at MKE (MSN), and were strictly a cold season occurrence. A listing of the cases so identified is provided in

Unauthenticated | Downloaded 05/10/21 09:57 PM UTC

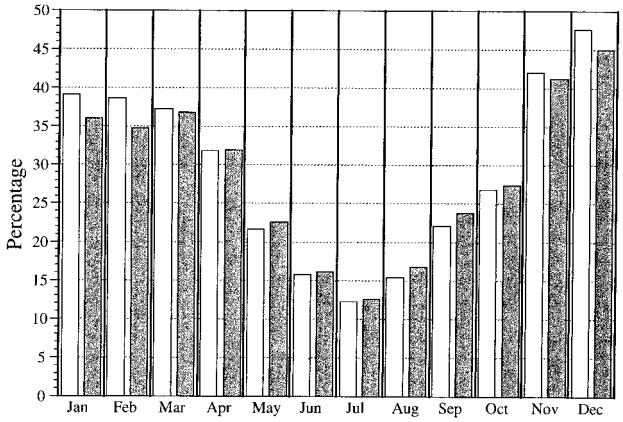

FIG. 2. The percentage of the hours in each month with low overcast conditions (100% cloud coverage with ceilings less than or equal to 2 km) at MKE (white bars) and MSN (gray bars). The analysis is based on the 1961–90 period, using 3-h surface reports.

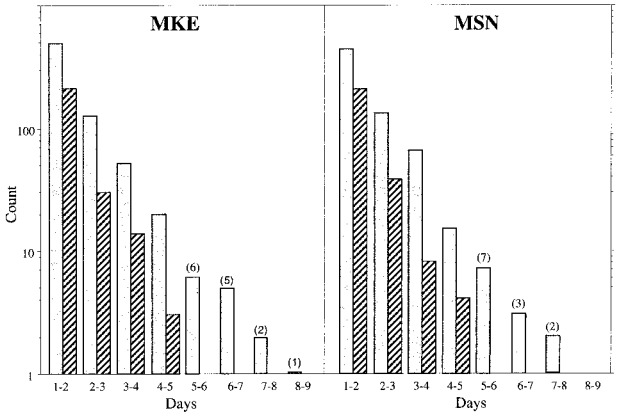

FIG. 3. The number of periods of continuous low overcast periods at MKE and MSN in the 1961–90 period, broken down by event length (days). Separate results are shown for the cold season (November–April, gray) and the warm season (May–October, hatched). The numbers in parentheses denote the count of the periods with lengths of at least 5 days. Note the logarithmic scale.

Table 2, along with the December 1991–January 1992 event, which will be studied in some detail in section 3. Cross-matching of the events at MKE and MSN indicates that there were a total of 18 such events affecting southern Wisconsin in the 1961–90 period. In fact, the low cloud conditions extended beyond this area, indicating that these events were not strictly local in character. This is not surprising, given their persistence, but it establishes that a synoptic or large-scale pattern is associated with their development, extending the applicability of this analysis to the wider region of the upper Midwest, and suggests that local controls are of secondary importance. This point will be further investigated through experiments with a simple PBL model in section 3.

b. Synoptic conditions associated with PLOEs

The regional character of PLOEs noted in section 2a provides motivation to investigate whether characteristic lower-tropospheric signatures are associated with their occurrence. As a preliminary step toward this goal, composite and anomaly patterns at 500 hPa, 850 hPa, and sea level were constructed (Figs. 4–7) for three especially long-lived episodes (identified by the asterisks in Table 2). Composite patterns were generated by averaging through each event once-daily observations (1200 UTC) from the National Centers for Environmental Prediction (NCEP, formerly the National Meteorological Center) Northern Hemisphere 381-km octagonal gridded dataset (Shuman and Hovermale 1968; Mass et al. 1987). The anomaly structures of the PLOEs were constructed by subtracting the climatological fields (derived from long-term monthly data) from each of the base composite patterns.

The composite flow pattern at 500 hPa for the December 1991–January 1992 PLOE is shown in Fig. 4a. This pattern can be compared to Figs. 4b and 4c, which show the composite patterns for the shorter-duration PLOEs of November–December 1987 and December 1972. In both the 1991–92 and 1987 cases, the strong composite 500-hPa Pacific jet splits over North America, with the southwesterly (northwesterly) subtropical (polar) jet positioned over the southern United States (northern Canada), leading to confluence downstream of the U.S. midwest. The anomalous nature of this split flow is indicated by the strong positive 500-hPa height

TABLE 2. Dates (in chronological order) of PLOEs (120 h or longer, bold type) in the period 1961–90 at MKE and MSN. The dates are expressed as start date–end date (YYMMDDHH format, with hours in UTC). The total consecutive hours of low overcast is enclosed in parentheses. In the case of a PLOE at only one of the two sites, the longest period of low overcast at the matching site during the PLOE is listed. Superscripts of A and B indicate events in which the large-scale circulation is subjectively similar to the 1991–92 and the 1972 PLOE, respectively. Asterisks beside the case numbers refer to cases for which further analysis was conducted.

Case	Dates at MKE	Dates at MSN
1	62030520–62031011 (111)^{A}	**62030808–62031417 (153)**^{A}
2	**62123111–63010511 (120)**^{A}	**62123123–62010817 (186)**^{A}
3	**65120923–65121623 (168)**^{A}	**65121005–65121520 (135)**^{A}
4	**67120611–67121217 (150)**^{A}	**67102523–67121217 (162)**^{A}
5*	**72121917–72122702 (177)**^{B}	**72121920–72122623 (171)**^{B}
6	**74011708–74012314 (150)**^{A}	**74011711–74012302 (135)**^{A}
7	75021508–75021917 (105)^{A}	**75021411–75021911 (120)**^{A}
8	80021911–80022402 (111)^{A}	**80021823–80022323 (120)**^{A}
9	**83121008–83121611 (147)**^{A}	**83121020–83121602 (126)**^{A}
10	**84031705–84032302 (141)**^{A}	84031820–84032217 (093)^{A}
11	85022114–85022608 (114)^{B}	**85022105–85022623 (138)**^{B}
12	**85110823–85111423 (144)**^{B}	85111117–85111423 (078)^{B}
13	**86013111–86020702 (159)**^{A}	**86013108–86020705 (165)**^{A}
14	**86021523–86022202 (135)**^{B}	86021602–86022023 (117)^{B}
15	**86122908–87010323 (135)**^{B}	**86122908–87010317 (129)**^{B}
16*	**87112414–87120217 (195)**^{A}	87112420–87112908 (108)^{A}
17	**87120517–87121017 (120)**^{A}	87120611–87121011 (096)^{A}
18	**87121208–87121708 (120)**^{B}	87121205–87121611 (102)^{B}
—*	**91122920–92011011 (280)**^{A}	**91123005–92011009 (268)**^{A}

Unauthenticated | Downloaded 05/10/21 09:57 PM UTC

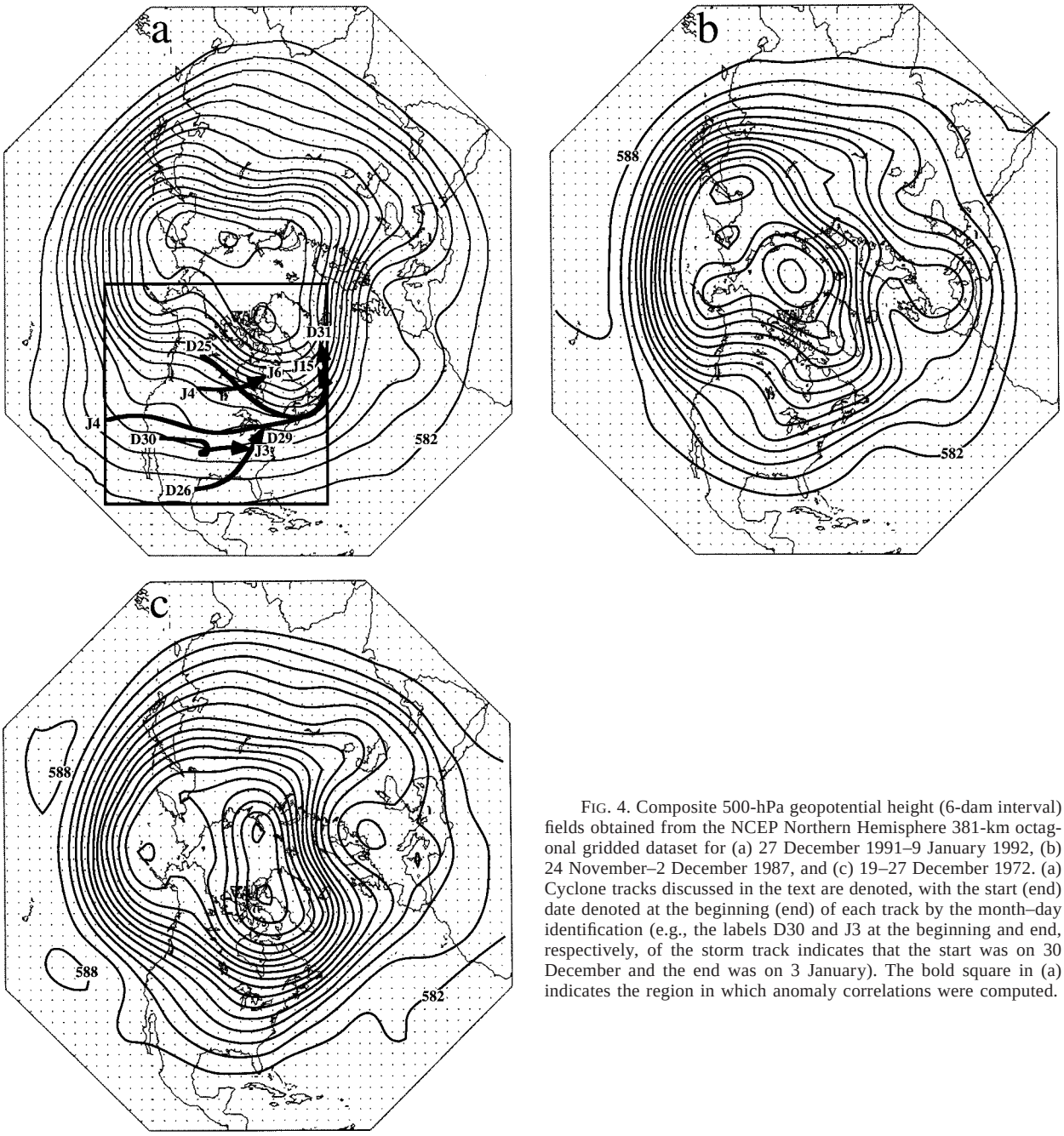

FIG. 4. Composite 500-hPa geopotential height (6-dam interval) fields obtained from the NCEP Northern Hemisphere 381-km octagonal gridded dataset for (a) 27 December 1991–9 January 1992, (b) 24 November–2 December 1987, and (c) 19–27 December 1972. (a) Cyclone tracks discussed in the text are denoted, with the start (end) date denoted at the beginning (end) of each track by the month–day identification (e.g., the labels D30 and J3 at the beginning and end, respectively, of the storm track indicates that the start was on 30 December and the end was on 3 January). The bold square in (a) indicates the region in which anomaly correlations were computed.

anomalies located over Canada (Figs. 5a and 5b). Correspondingly, composite surface conditions (Figs. 6a–d) were relatively quiescent with broad-scale high pressure centered over the upper Great Lakes and anticyclonic flow affecting most of the eastern two-thirds of the United States. However, the flow in 1972 was substantially different (Figs. 4c, 5c, 6e and 6f). In this case, the composite flow was quite zonal with a 20 m s^{-1} westerly geostrophic jet at 500 hPa (compared to 12.5 m s^{-1} in 1991–92 and 1987), suggesting an active weather pattern with more rapid progression of synoptic-scale cyclones and anticyclones. This anomalous westerly jet is marked by the zonally elongated positive (negative) 500-hPa height anomaly centers across the United States (Canada) in Fig. 5c. In fact, four cyclones affected (i.e., had an observable effect on sensible weather elements) the Midwest during the approximately 7 days of the 1972 PLOE. There were also four cyclones that affected the Midwest in the 1991–92 event, but over a time span twice as long. The differences between 1991–

Unauthenticated | Downloaded 05/10/21 09:57 PM UTC

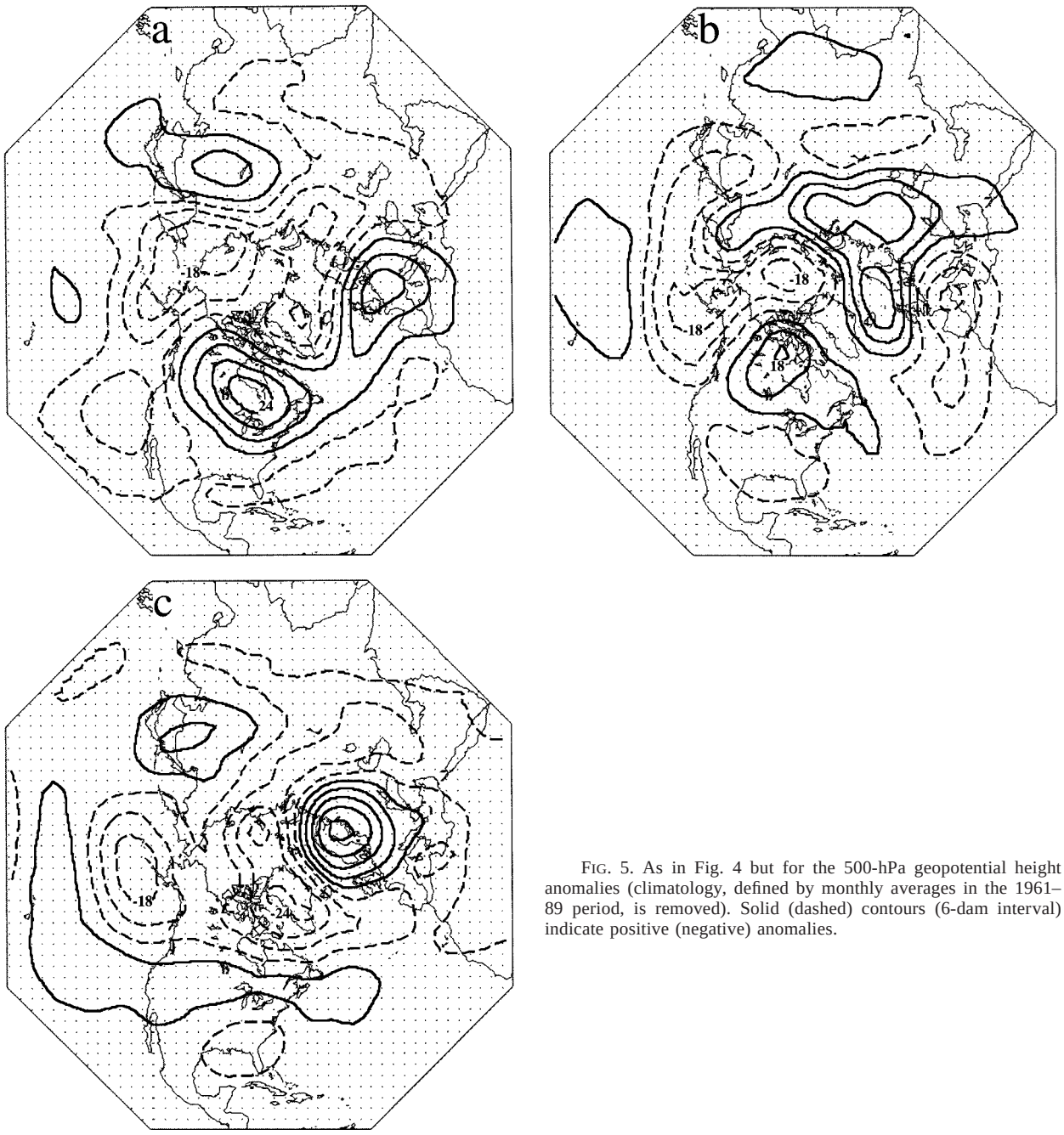

FIG. 5. As in Fig. 4 but for the 500-hPa geopotential height anomalies (climatology, defined by monthly averages in the 1961–89 period, is removed). Solid (dashed) contours (6-dam interval) indicate positive (negative) anomalies.

92 and 1987, and 1972 are also reflected in the sea level pressure anomaly charts for these times (Figs. 6b and 6d versus Fig. 6f, respectively); in the former cases, anomalously high sea level pressure is the rule over the eastern two-thirds of North America, whereas in the latter, an anomalous trough extends from the Pacific coast southeastward across the Great Lakes basin. Visual inspection of the 500-hPa and sea level maps for the 18 cases listed in Table 2 revealed that the majority of the identified events (12) occurred in regimes qualitatively similar to that of the 1991–92 PLOE, with the remainder developing under patterns like that of the 1972 PLOE.

Since the 850-hPa level provides the closest measure of the flow within the cloud layer for these cases (where cloud bases remain confined below 2 km), we show charts for this level in Fig. 7. The broad similarity between the three cases at this level is notable, with a composite trough positioned over the Midwest in the westerly flow (Figs. 7a, 7c and 7e). There is a clear

Unauthenticated | Downloaded 05/10/21 09:57 PM UTC

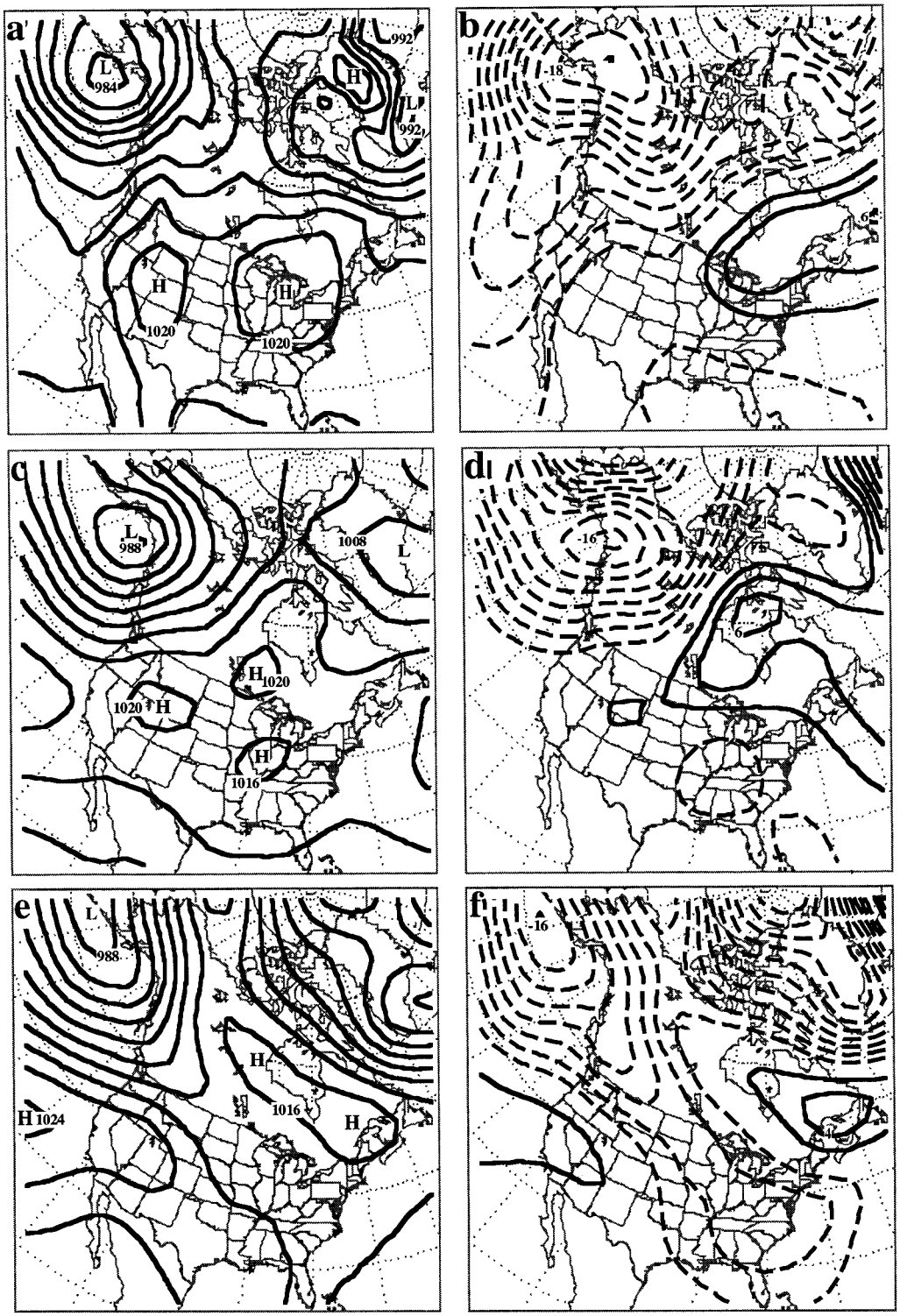

FIG. 6. Composite sea level pressure (4-hPa interval) and anomaly fields obtained from the NCEP Northern Hemisphere 381-km octagonal gridded dataset for the 3 PLOE events. Sea level pressure (a) and anomaly (b) for 27 December 1991–9 January 1992, sea level pressure (c) and anomaly (d) for 24 November–2 December 1987, and sea level pressure (e) and anomaly (f) for 19–27 December 1972.

Unauthenticated | Downloaded 05/10/21 09:57 PM UTC

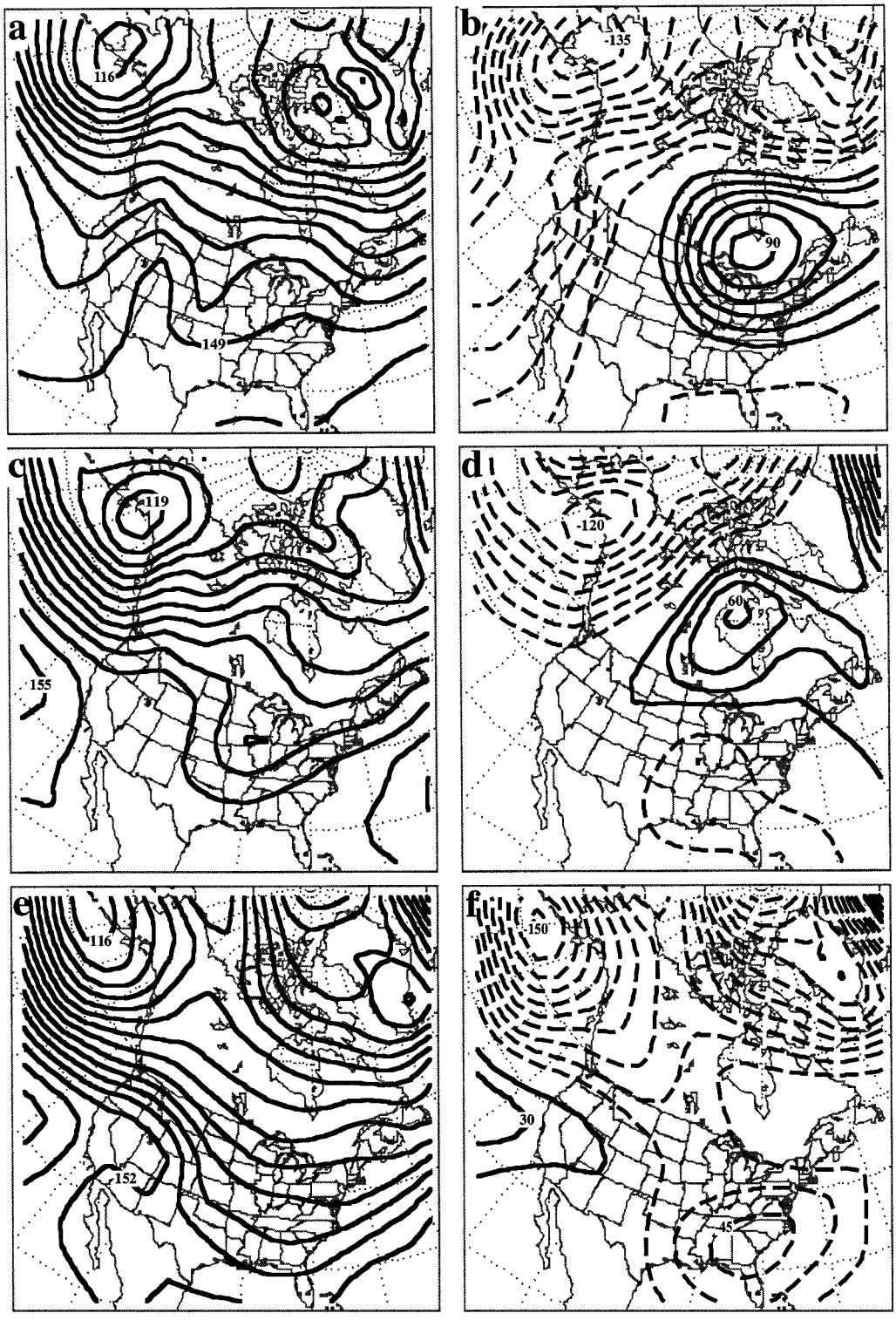

FIG. 7. As in Fig. 6 but for 850 hPa.

Unauthenticated | Downloaded 05/10/21 09:57 PM UTC

transition in the ''weight'' of the signed anomalies between the 1991–92 case and 1972 (Figs. 7b and 7f), with the former (latter) being dominated by above normal (below normal) heights in southeastern and central Canada (the southeastern United States). However, in each case the anomaly patterns exhibit anomalous easterly flow across the upper Midwest, indicating weaker than normal horizontal airflow near the cloud layer. In order to perform such comparisons on a more rigorous basis, we will compute regional anomaly correlations for all three levels (500 hPa, 850 hPa, and sea level) as described in the next section.

c. Observations from PLOE analogs

The qualitative conclusions of section 2b suggest the utility of quantifying the extent of the similarity between large-scale signatures of PLOEs. Accordingly, we have searched the period from 1961 to 1989 (using data archived on the NCEP 381-km octagonal grid) for analogs to the 1991–92 flow at 500 hPa, 850 hPa, and sea level. Since Lorenz (1969) convincingly demonstrated the futility of searching for hemispheric analogs within the foreseeable future, a regional analog procedure (Roebber and Bosart 1998) was employed as follows:

1) 1200 UTC 500- and 850-hPa height and sea level pressure patterns for each day in the 1961–89 period and for each of the subsequent four days were composited;
2) the climatological pattern at each of these levels was subtracted out to leave the composite anomaly pattern for each 5-day period, where $a_{i,j}$ is the anomaly at a particular grid point (i, j) defined by

$$a_{i,j} = z_{i,j} - \overline{z_{i,j}}, \quad (1)$$

where $z_{i,j}$ represents the geopotential height or pressure at the grid point and the overbar denotes the climatological average value at that point (defined from long-term monthly data);
3) the anomaly correlation (AC) of each date with the 1991–92 PLOE was computed within a 21 × 21 gridpoint region of the NCEP 381-km octagonal gridded data, according to

$$\mathrm{AC} = \frac{\sum_i \sum_j a\{1\}_{i,j} a\{2\}_{i,j}}{\sqrt{\left(\sum_i \sum_j a\{1\}_{i,j}\right)^2 \left(\sum_i \sum_j a\{2\}_{i,j}\right)^2}}, \quad (2)$$

where $a\{1\}$ and $a\{2\}$ denote the anomalies from the 1991–92 case and the potential analog, respectively. The bold outline in Fig. 4a shows the region within which the ACs were computed.

Hollingsworth et al. (1980) found that AC values above 0.5–0.6 yield patterns that are sufficiently similar to be useful for synoptic interpretation. The results of this procedure (Table 3) show that the similarity of the 1987 and 1991–92 large-scale flow regimes (AC = 0.7376, 0.7368, and 0.6704 at 500 hPa, 850 hPa, and sea level, respectively) extends beyond the qualitative correspondence of many of the cases listed in Table 2. Furthermore, a number of other long-duration low overcast episodes, which were insufficient in length to qualify as PLOEs based on the 120-h standard, occurred in conjunction with this type of flow (December 1979, October 1984, December 1986). However, in several instances, rigorous circulation analogy with the 1991–92 PLOE did not produce extensive periods of low overcast (October 1963, September 1966, September 1967, November 1979, January 1981, November 1983). Thus, flow similarity to the 1991–92 event, although common (8 of the 18 cases listed in Table 2 had AC > 0.5 for at least one of the three levels examined), is neither a necessary nor a sufficient condition for the development of PLOEs in the upper Midwest. We shall return to this point in the concluding discussion (section 4). In order to document the physical processes operative in such episodes, we turn to a detailed analysis of the 1991–92 event in the next section.

TABLE 3. Five-day composite AC between the 1991–92 PLOE and all days in the 1961–89 period. Listed are the 10 highest dates, based upon a combined rank score for the 500-hPa, 850-hPa, and sea level AC. Also shown is a summary of the continuous low overcast conditions (hours) experienced at MKE during each period. Dates are for the start of the 5-day composite period and are expressed in YYMMDD format. Figure 4a shows the region within which the AC was calculated.

Date	AC (500 hPa)	AC (850 hPa)	AC (sea level)	Continuous low overcast
831102	0.8060	0.7981	0.7608	27 h
841007	0.7351	0.7516	0.7781	63 h, 9-h break, 96 h
660917	0.6664	0.8256	0.8373	27 h
861224	0.6404	0.7551	0.7822	111 h
631019	0.6323	0.7489	0.7363	24 h
670910	0.6523	0.7312	0.7206	No continuous low overcast
810114	0.6719	0.6926	0.7254	54 h
871125	0.7376	0.7368	0.6704	195 h
791119	0.6918	0.6858	0.6875	42 h
791218	0.7102	0.6794	0.6629	102 h

3. The December 1991–January 1992 PLOE

The basic large-scale character of this PLOE was shown in section 2 (Figs. 4a, 5a, 6a and 6b, and 7a and 7b). Figure 8 presents the time series of surface observations (sea level pressure, temperature, dewpoint, wind, cloud amount and ceiling) at MKE for this period. The strict definition of a PLOE outlined in section 1 requires that this episode be considered to have begun at 2000 UTC 29 December 1991, continuing for the next 280 h (nearly 12 days) through 1100 UTC 10 January 1992. However, low overcast conditions at MKE began at 1700 UTC 26 December 1991 and were interrupted during the next 15 days only by a 5-h period

Unauthenticated | Downloaded 05/10/21 09:57 PM UTC

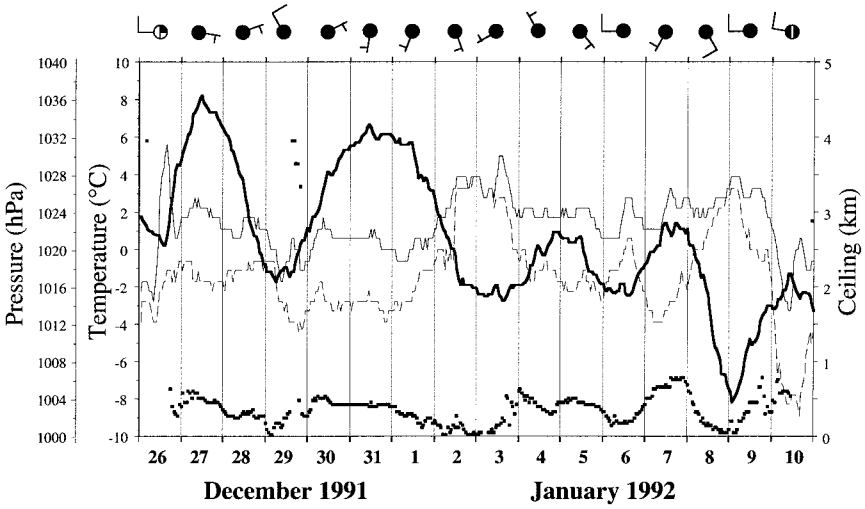

FIG. 8. Hourly time series of sea level pressure (hPa, bold), temperature (°C, thin solid), dewpoint temperature (°C, thin dashed), and ceiling height (km, filled squares) at MKE in the period 0000 UTC 26 December 1991–0000 UTC 11 January 1992. Also shown are the 24-h average wind (long barb 5 m s^{-1}, short barb 2.5 m s^{-1}) and cloud coverage, following the standard station model.

of elevated overcast (ceiling heights lifted to 3–6 km) on the morning of 29 December. In sections 3a–c, we will introduce the analysis techniques that will be used to study the physical processes governing the evolution of this event, while in section 3d, we present the results of those analyses.

a. Analysis of rawinsonde data

In order to better understand the vertical structure of the atmosphere during this period, rawinsonde data from five locations in the upper Midwest (Fig. 1) were examined: Green Bay, Wisconsin (GRB); Flint, Michigan (FNT); Dayton, Ohio (DAY); St. Cloud, Minnesota (STC), and Peoria, Illinois (PIA). These data were used directly to examine the regional character of atmospheric profiles of temperature, moisture, and wind and indirectly to diagnose dynamical (divergence and vertical motion) and moisture budget characteristics following the triangulation techniques of Bellamy (1949) and Bosart and Sanders (1981). With the assumption that all condensed water falls out of the atmospheric column as precipitation, the excess of precipitation (P) over evaporation (E) within a triangle (where the sounding stations are positioned at the vertices of the triangle; see Fig. 1) can be written as

$$\overline{P-E} = -\sum_{i=1}^{3} \frac{1}{h_i} \int_{100\,\text{mb}}^{\overline{p}\,(\text{sfc})} q_i v_{h_i} \frac{dp}{g} - \frac{\partial}{\partial t} \int_{100\,\text{mb}}^{\overline{p}\,(\text{sfc})} \overline{q}\, \frac{dp}{g}. \quad (3)$$

Here, q is the specific humidity, h is the altitude (length) from the triangle vertex to the opposite side, and v_h is the wind component at the vertex directed outward and parallel to h. An overbar denotes an average over the area of the triangle, and the summation is over each of the three triangle vertices.

The first term on the right-hand side of (3) represents the vertical integral of the water vapor flux transport ($-\overline{\nabla \cdot qV}$), which can be partitioned into the horizontal advection of water vapor ($-\overline{V \cdot \nabla q}$) and convergence in the presence of water vapor ($-\overline{q \nabla \cdot V}$). While the vapor flux divergence term is itself an easily understood process, this split was made to explicitly separate advective processes from moisture divergence, which often result from distinct physical forcings (e.g., a broad southerly flow with a small Laplacian of warm air advection producing little low-level convergence but ample moisture advection; strong differential cyclonic vorticity advection producing low-level convergence in the presence of moisture with little attendant moisture advection). These terms were time averaged over two successive sounding intervals (12 h). The second term on the right-hand side of (3) represents the local time rate of change of atmospheric precipitable water ($-\partial \overline{W}/\partial t$), computed as the change over the same 12-h period as the above averaging, and measures the storage of precipitable water. The vertically integrated divergence profiles were corrected to zero by means of a linear correction factor (O'Brien 1970) and were then used to diagnose the vertical velocity profile. The STC–PIA–GRB and PIA–DAY–GRB triangles shown in Fig. 1 (because of missing wind data, FNT could not be used in the triangle calculations for this case) represent areas west and east, respectively, of MKE. Vertical motions and moisture budget term derived from these triangles are areally weighted and thus represent regional measures of these quantities.

Unauthenticated | Downloaded 05/10/21 09:57 PM UTC

b. Estimates of evaporation

Given observations of precipitation, it is possible to diagnose surface evaporation as a residual term in (3). However, because evaporation may be an important effect in this case and since the residual will include potentially large error effects as well as the desired signal, we have chosen instead to compute surface evaporation from the available surface observations using similarity theory as described in the PBL formulation of Blackadar (Blackadar 1976; 1979; Zhang and Anthes 1982). In this formulation, the boundary layer is characterized according to the bulk Richardson number (R_{iB}) given by

$$R_{iB} = \frac{gz_a}{\theta_a}\frac{\theta_{va} - \theta_{vg}}{V^2}, \quad (4)$$

where the subscripts g and a refer to the ground, the atmospheric layer closest to the ground, and v denotes the virtual temperature correction, respectively; θ is the potential temperature; and V is the wind speed in the surface layer. For the conditions of the period under study, two boundary layer cases are possible: stable ($R_{iB} > 0.2$) or mechanically driven turbulence ($0 \leq R_{iB} \leq 0.2$). In each case, surface moisture flux is determined following Carlson and Boland (1978) by

$$E_s = M\rho I^{-1}(q_{vs} - q_v), \quad (5)$$

where M is the moisture availability (which varies from 1.0 for a water surface to 0.0 for a surface with no potential for evaporation), ρ is the density of air, q_v (q_{vs}) is the specific (saturation specific) humidity, and the parameter I is defined by

$$I^{-1} = ku_*\left[\ln\left(\frac{ku_*z_a}{K_a} + \frac{z_a}{z_1}\right) - \varphi_h\right]^{-1}, \quad (6)$$

where k is the von Kármán constant, z_1 is the depth of the molecular layer, and K_a is the background molecular diffusivity. The friction velocity u_* is determined by

$$u_* = 0.1 \text{ m s}^{-1} \quad \text{(stable)}$$

$$= \text{MAX}\left(\frac{kV}{\ln\frac{z_a}{z_0}}, 0.1 \text{ m s}^{-1}\right) \quad \text{(mechanical)}, \quad (7)$$

where z_0 is the roughness length. Since direct observations of the ground temperature were not available, it was assumed that except under calm wind conditions, $R_{iB} = 0$ and that the mechanically driven turbulence regime would apply. Given this assumption. the nondimensional stability parameter φ_h is determined by

$$\varphi_h = -10 \ln\frac{z_a}{z_0} \quad \text{(stable)}$$

$$= 0 \quad \text{(mechanical)}. \quad (8)$$

As indicated by (5), surface wind speed, vertical moisture gradients, and moisture availability all control the magnitude of the surface moisture flux. For the latter variable, no direct measurements are available. We have assumed that $M = 1.0$, given that a light snow cover was in place at the beginning of the period and that measurable precipitation fell at MKE on 2, 8, and 9 January [see Oncley and Dudhia (1995) for some justification of this approach]. Thus, 12-h evaporation amounts obtained through (5) with these assumptions should be considered as an upper limit to that which actually occurred. Values for all the parameters used in (4)–(8) are listed in Table 4.

TABLE 4. Parameter values used to determine evaporation from Eq. (5).

Parameter	Symbol	Value
Measurement level	Z_a	10 m
Moisture availability	M	1.0
Von Kármán constant	k	0.4
Background molecular diffusivity	K	2.4×10^{-5} m^2 s^{-1}
Depth of molecular layer	z_1	0.01 m
Roughness length	z_0	0.05 m
Friction velocity	u_*	0.1 m s^{-1} (stable) Eq. (7) (mechanical)

c. PBL modeling

The procedures detailed in sections 3a and 3b will give considerable information on synoptic and regional controls for this event. However, in order to gain a deeper understanding of the role of boundary layer processes (which are governed by a wide variety of variables and their interactions), sensitivity experiments are required. Accordingly, we have modeled the evolution of the GRB soundings for this PLOE in 12-h segments by integrating a one-dimensional time-dependent implementation of the Blackadar PBL formulation [see Blackadar (1997) for a detailed description of and code for this model].

In this version, the PBL is simulated by considering a 10-m-thick surface atmospheric layer (where Monin–Obukov similarity is assumed) and 30 additional layers of 100-m depth (where K theory is applied except under conditions of free convection) extending to 3 km above ground level. Within the surface layer lies a vegetative layer that interacts with the radiative fluxes and, through diffusion, with the surface layer. A two-layer ground-slab model of the soil is applied; the deep-soil layer is maintained at a constant temperature and water content (an infinite heat reservoir or sink) while surface temperatures are computed from a surface energy budget following the force–restore method. Much of the soil of southeastern Wisconsin is silt loam (e.g., Schultz 1986), which was estimated to be one-half clay and one-half sand, so a weighted average of the heat capacities of these two materials [1.42×10^6 J m^{-3} and 1.28×10^6 J m^{-3}, respectively; see Oke (1978, p 38)] was used to determine a dry soil heat capacity of 1.35×10^6 J m^{-3}.

Unauthenticated | Downloaded 05/10/21 09:57 PM UTC

TABLE 5. Blackadar PBL model parameters used in the simulations of the GRB soundings in the period 0000 UTC 26 December 1991 to 0000 UTC 11 January 1992.

Parameter	Value
Latitude	44.48°N
Solar declination	Computed for each date except for artificial summer runs (23.4°)
Mean middle–high cloudiness	0%
Precipitable water	Computed from rawinsondes
Soil albedo	0.4675
Dry soil heat capacity	1.35×10^6 J m^{-3}
Surface roughness	0.05 m
Subsidence	Vertical motion computed from triangles at 850 hPa, except for strong subsidence (5 cm s^{-1}) runs
Vegetation	75% coverage
Albedo of vegetation	0.20
Leaf area index	0.001
Soil water field capacity	660 kg m^{-3}
Soil water wilting threshold	300 kg m^{-3}
Saturation water content of vegetation	0.002 kg m^{-2}

Model data and parameters (see Table 5) are initialized by reading an input file derived from the GRB soundings. In the 30 atmospheric layers, heat, water, and momentum budgets are kept and updated at 2-min intervals. The horizontal transport of heat can be accounted for by the vertical shear of the geostrophic wind, which through thermal wind balance yields an implied temperature change. However, since the actual wind shear in the lower portion of the atmosphere is affected by processes that may violate thermal wind balance, this implied temperature change is subject to some error. For the two time periods where strong temperature advections may have been contributing factors to the cloud breakup (see Fig. 8), the sensitivity of our results to this factor was tested and will be noted below. If supersaturation occurs during a model simulation the excess moisture is condensed out and a cloud is displayed at the appropriate level. The transmissivity of incoming solar radiation (the ratio, for vertical incidence, of the transmitted direct solar beam intensity to that entering the top of the atmosphere) is modified by these (stratiform) clouds, which are assumed to cover the whole sky. Rising thermals that become supersaturated form cumulus clouds; however, these clouds are not considered to cover a significant proportion of the sky and radiative interactions are thus ignored (it should be remembered that for the conditions of this case, cumulus effects are not a consideration). Model results are output at 10-min intervals; these results include, in addition to low cloud, vertical profiles of temperature, dewpoint and wind, and the surface heat balance terms (net radiation, heat storage in the ground, and sensible and latent heat fluxes to the atmosphere).

Since the atmosphere is not simulated above 3 km, important properties above this level must be specified. For example, the specified values of mean high and middle cloudiness are used to compute the transmissivity of shortwave radiation. Precipitable water is used to calculate the downward IR radiation at the 3-km level. A free-atmospheric subsidence rate (ranging from 0 to 5 cm s^{-1}) must also be specified since this in part determines adiabatic temperature changes. In these simulations, the subsidence rate was obtained directly from the triangle calculations of vertical motion. The model also provides an option to turn off infrared radiative transfer, whose effects can be important when clouds are present. Unless otherwise stated, infrared radiative transfer is switched on in the simulations.

Surface characteristics in addition to soil properties (albedo, surface roughness, vegetative properties) are also important. Based on land use in southern Wisconsin, the surface albedo was determined by areally averaging between urban (25% of the area, considered as snow free) and rural (75% of the area, snow covered) albedo values. The albedo of the light, old snow cover (the last snowfall was 2.3 cm on 20 December) was taken as 0.55 (Arya 1988) while the urban albedo was set to 0.22, giving a regional albedo of 0.4675. We note that this may represent an overestimate of the *time-dependent* albedo, as the light rain that fell on several days during the PLOE would likely have reduced it further. As in the above calculations of evaporation (section 3b), the surface aerodynamic roughness (the height at which the wind speed profile in the surface projects to a speed of zero) was set to a rural value of 5 cm.

The water transfer from the soil is strongly influenced by the presence of vegetation and is modeled following an expanded version of the scheme used by Deardorff (1978). The sensitivity of the case to soil moisture content can be assessed by varying the soil moisture between two well-defined limits: the wilting threshold (the water content at which capillary tension becomes so high that roots are unable to extract water from the soil) and the field capacity (the upper limit of water that a particular soil can hold, with the excess simply running off the surface). Values derived from Sellers (1965) were used and are listed in Table 5. Because this is a cold season case and much of Wisconsin is covered by deciduous trees, the leaf area index (LAI), the total one-sided leaf area situated above a unit area of the vegetated portion of the earth's surface, was set to a negligible value. Likewise, the water content of the vegetation, which is produced by multiplying the water saturation coefficient of the vegetation by the LAI, was negligible for this case.

d. Analysis results

A comparison of 12-h forecasts from the PBL model ''control'' simulations with the observed atmospheric structure (potential temperature and relative humidity) in the lowest 3 km is presented in Figs. 9a and 9b. In general, the greatest temperature and moisture errors

Unauthenticated | Downloaded 05/10/21 09:57 PM UTC

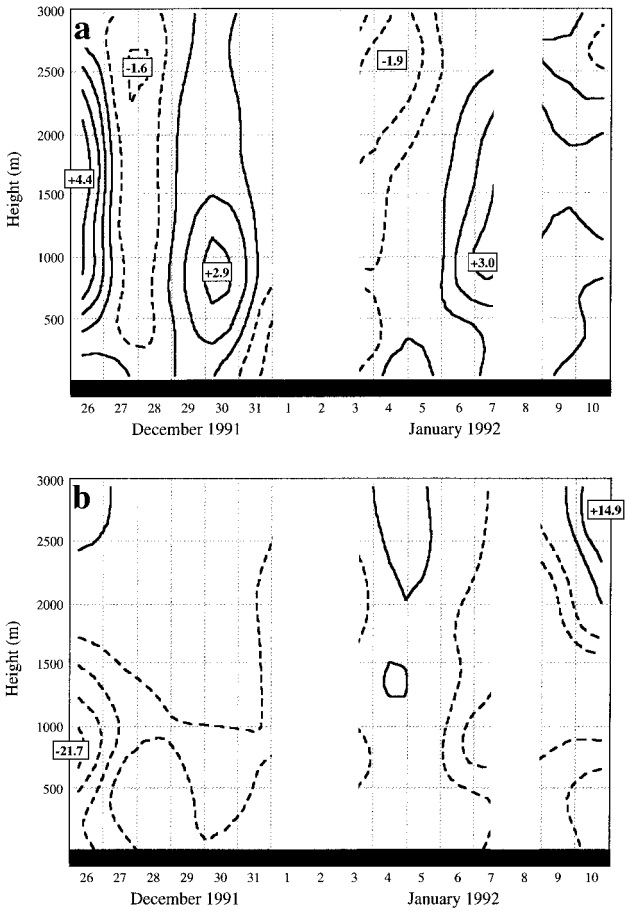

FIG. 9. Time–height cross section for the period 0000 UTC 26 December 1991–0000 UTC 11 January 1992 of difference fields of Blackadar PBL simulations for (a) control minus observed, potential temperature (1°C interval), and (b) control minus observed, relative humidity (5% interval). Solid (dashed) contours indicate positive (negative) values. Breaks in the analysis indicate periods in which deep tropospheric ascent was occurring, invalidating the PBL model simulations.

occur directly above the cloud layer in association with simulations that are too warm and dry (temperature errors at the 1.5-km level over the event are 0.7°C bias and 2.8°C std dev). Dimego et al. (1992) found that 12-h temperature forecast errors from the NCEP operational model at 850 hPa (near 1.5 km) were 0.0°C bias and 2.0°C std dev. Thus, the PBL model errors are likely somewhat larger than the average operational model errors of the time (although it should be noted that the NCEP model errors are not computed on the basis of a specific event type).

One limitation of applying a 1D PBL model in the present study is its inability to simulate potentially important horizontal advections of moisture. This limitation is partially controlled by initializing the model integrations with data from the GRB soundings every 12 h, since any drift in the vertical profile of moisture caused by such unspecified advections will be erased in the subsequent initialization. The warm and dry bias indicated in Figs. 9a and 9b appears to reflect the model sensitivity to the magnitude of the specified free-atmospheric subsidence rate rather than problems with horizontal advections of moisture. This is due in part to the fact that the model was not run for periods in which deep tropospheric ascent was occurring, since such ascent would invalidate a basic model assumption (zero or sinking vertical motion). Such ascent frequently occurs in conjunction with strong horizontal transport of moisture (e.g., 2 and 8 January; see Fig. 12). In order to check the sensitivity of the model to subsidence, the simulation was rerun with the diagnosed subsidence replaced with a fixed value of 5 cm s^{-1}, representing strong sinking. The results of this experiment, averaged over the entire PLOE period, are displayed by the curves labeled SUB in Figs. 10a and 10b. The obvious sensitivity of the model to the specified subsidence suggests that the temperature and moisture errors in the control simulation could be further reduced by using the predicted vertical motions from the operational models rather than as diagnosed from the relatively crude triangle technique. Since the control simulation errors (with respect to the observations at GRB) are tolerably small, these results suggest the applicability of the PBL model to forecast problems (where the model might be used as a tool to enhance the capabilities of forecasters whose basic guidance would be provided by the NCEP models) as well as to the diagnostic purpose employed here. Accordingly, we shall proceed in this study without further adjustment of these inputs.

A time–height (pressure) cross section (Fig. 11) showing potential temperature, relative humidity, and vertical motion (obtained from the triangulation procedure described in section 3a) was constructed from the rawinsonde observations at GRB for 26 December 1991 through 10 January 1992. The moisture budget terms of (3) are presented for the same period in Fig. 12. Although the composite 500-hPa geopotential height field suggests quiescent conditions in the upper Midwest during this 15-day interval (as suggested by the composite splitting of the flow north and south of the region; Fig. 4a), inspection of Figs. 8 and 11 reveal that this period was in fact punctuated by several structural transitions. On 25 December 1991, a cyclone originating to the lee of the Canadian Rockies propagated east-southeast along the polar jet stream (storm track labeled D25–D31 in Fig. 4a). On 26 December, this cyclone advanced north of Lake Superior and a trough line extending southwestward from the cyclone center passed through Wisconsin (see also Fig. 14a), followed by rising pressures and the onset of low overcast conditions at MKE (Fig. 8). Strong high pressure remained entrenched over Wisconsin until 29 December and this period was characterized by a strengthening of the subsidence inversion and trapped low-level moisture (Fig. 11). Surface analyses (not shown) and *Geostationary Operational Environmental Satellite-7* (*GOES*-7) 2-km resolution vis-

Unauthenticated | Downloaded 05/10/21 09:57 PM UTC

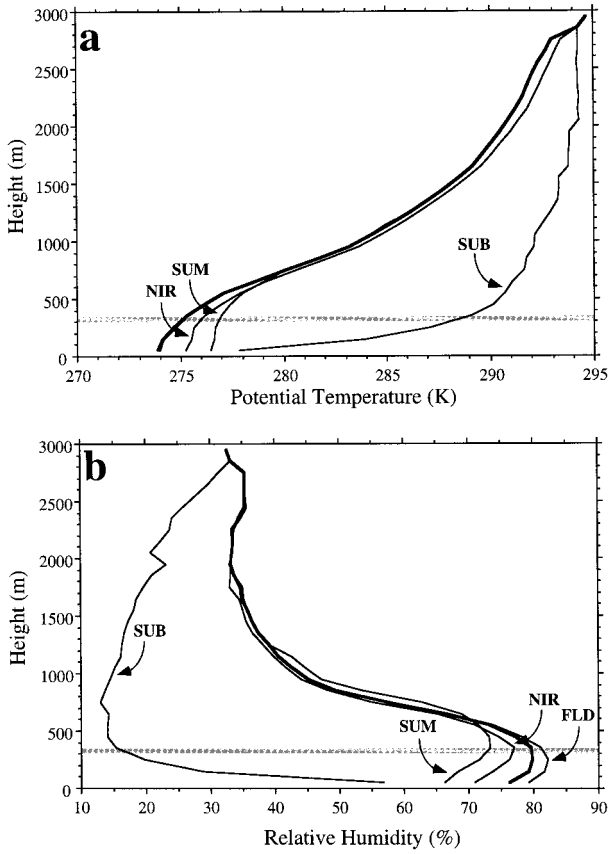

FIG. 10. Vertical profiles of (a) potential temperature (K) and (b) relative humidity (%) for the control PBL simulation (thick line) and a series of sensitivity experiments, averaged over the period 0000 UTC 26 December 1991–0000 UTC 11 January 1992 (times not plotted in Fig. 9 were not averaged). In the sensitivity experiments, parameter settings were identical to those of the control, with the exception of the parameter under study. The sensitivity experiments were NIR, no infrared radiative transfer; SUM, solar declination set to a summer value (23.4°); SUB, strong free-atmospheric subsidence (5 cm s^{-1}); and FLD, soil moisture set to the field capacity. Note that in (a) the FLD experiment yielded a potential temperature profile indistinguishable from that of the control. The gray bar in the figures denotes the average level of the cloud base at MKE during this period.

ible imagery (Fig. 13) establish that the cloud deck was widespread, extending north to the upper peninsula of Michigan, east and south to the mid-Mississippi and Ohio River Valleys, and west to the Dakotas. The main positive contributors to the moisture budget during this time were surface evaporation and moisture advection in the easterly flow (Fig. 12). PBL model simulations of this time period with soil moisture set to the field capacity suggest that surface evaporation may have enhanced the cloud development (see the curve labeled FLD in Fig. 10b); however, low cloud developed, albeit later, in simulations in which soil moisture was set to the wilting threshold. Simulations with no subsidence (not shown) resulted in no inversion becoming established, or if a preexisting inversion was present, no further development of the inversion, but again low cloud developed. Thus, moisture advection appears to have been the primary agent in establishing the low overcast during this early period.

As a means to investigate the moisture transport within the cloud layer at key times during the PLOE, an analysis of the 950-hPa streamlines and surface to 900 hPa precipitable water was constructed (Fig. 14). The analysis for 1200 UTC 26 December (Fig. 14a) shows the plume of moisture associated with the southerly flow in the warm sector of the cyclone (north of Lake Superior) that initiated the event. By 0000 UTC 28 December (Fig. 14b), the easterly flow noted above had become established across the upper Midwest with anticyclones positioned along the upper Great Lakes. Since a ridge of precipitable water persisted along a line from Tennessee northward through Lakes Michigan and Superior, the easterly flow effectively advected higher moisture air westward into the study region. An interesting aspect of this case, beyond the scope of the present study (but addressable with a regional numerical weather prediction model such as the Pennsylvania State University–NCAR mesoscale model), relates to the role of the Great Lakes basin in maintaining this moisture ridge.

A weak cyclone that had originated ahead of a lifting 500-hPa trough embedded in the subtropical jet stream passed east of Michigan on 29 December (see storm track labeled D26–D29 in Fig. 4a; the cyclonic flow in the Gulf of Mexico in Fig. 14b) and the cold, dry advection in its wake led to a short-lived lifting of the cloud ceiling (Figs. 8 and 11). The effects of temperature advection were important in this period, as evidenced by PBL simulations with and without implied temperature changes. In the former case, the modeled sounding was drier and cloud ceilings were elevated compared to the run with no temperature advection. Thus, the early period was quite sensitive to forcing from synoptic-scale systems: a strong cyclone–anticyclone couplet with correspondingly strong vertical motion patterns would likely have destroyed the basic conditions responsible for the onset of the PLOE. This statement is further reinforced by additional simulations with the PBL model with strong subsidence (5 cm s^{-1}) replacing the weak (diagnosed) sinking motion that marked the reestablishment of surface high pressure on 30–31 December. As noted above, simulations with the diagnosed subsidence (Figs. 9a and 9b) were biased slightly too warm and dry, while the strong subsidence case was marked by a substantial drying (a drop in relative humidity of ~65% in the cloud layer relative to the control run; see Fig. 10b) and thinning of the moist layer until a complete breakup of the cloud ensued.

Surface high pressure remained in place until 1 January 1992, when a weak cyclone associated with a cutoff 500-hPa low embedded in the subtropical jet stream (see storm track labeled D30–J3 in Fig. 4a; cyclonic flow in Fig. 14c) began to approach the Midwest. At this time, the subsidence was replaced by weak ascent below 500

Unauthenticated | Downloaded 05/10/21 09:57 PM UTC

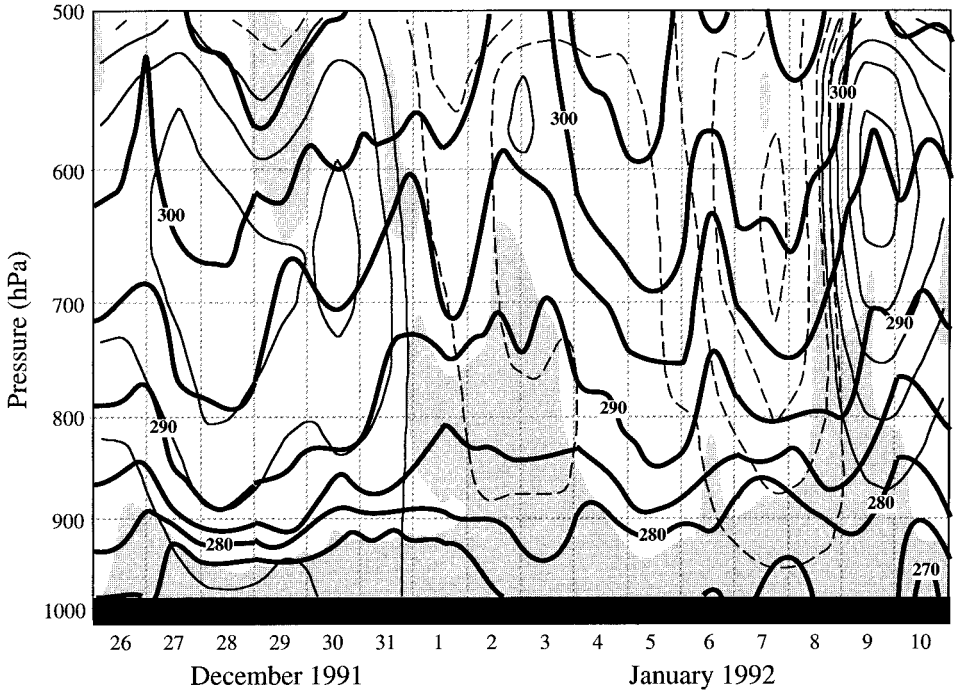

FIG. 11. Time–pressure cross section of potential temperature (bold, 5 K interval), relative humidity ≥ 70% (shaded), and vertical velocity (thin solid descent, thin dashed ascent, 10^{-1} Pa s^{-1} interval) at GRB for the period 0000 UTC 26 December 1991–0000 UTC 11 January 1992.

hPa (Fig. 11), and the southerly flow began transporting additional moisture into the upper Midwest (Figs. 12 and 14c). The trapping inversion was removed but the moist layer was augmented, leading to relative humidities in excess of 70% extending above the 700-hPa level (Fig. 11). Measurable precipitation (2.8 mm) was reported at MKE on 2 January.

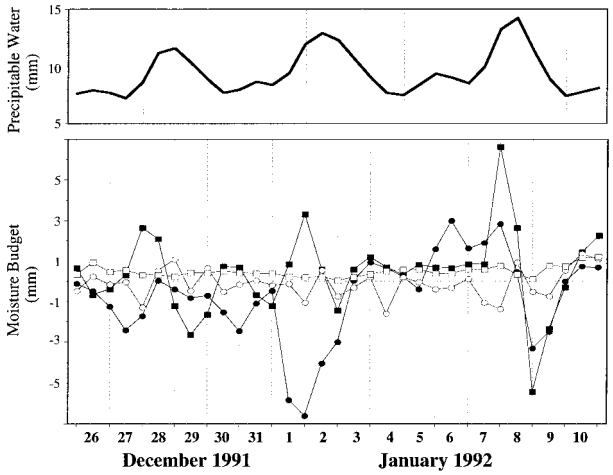

FIG. 12. Time series of moisture budget terms and precipitable water based on areally averaged values for the STC–PIA–GRB and PIA–DAY–GRB triangles (except surface evaporation, determined from similarity theory and the MKE surface data; see text for details) for the period 0000 UTC 26 December 1991–0000 UTC 11 January 1992. Shown are convergence in the presence of water vapor ($-\overline{q}\overline{\nabla}\cdot\overline{V}$, filled circles), moisture advection ($-\overline{V}\cdot\overline{\nabla}\overline{q}$, filled squares), precipitable water storage ($-\partial\overline{W}/\partial t$, open circles), and surface evaporation (E, open squares).

Surface high pressure became reestablished on 4 January following the passage of the cyclone and weak subsidence with a trapping inversion redeveloped in the lower troposphere (Fig. 11). PBL model experiments suggest that during the moisture augmentation period of 2 January, strong subsidence would again have resulted in the breakup of the cloud whereas by 4 January, this subsidence would have acted only to amplify the inversion, trapping this additional moisture at the lowest levels. Throughout this period, the effects of surface evaporation (as diagnosed through comparisons of PBL model runs with the soil moisture set to the field capacity with the control runs; see curves labeled FLD in Fig. 10b) are limited in scope; some additional moisture at low levels is realized in comparison to simulations with more limited soil moisture available (the wilting threshold case designated in the control), but in both instances low overcast is produced.

On 6–7 January, a weak cold front extending southwestward from a surface cyclone in Hudson Bay (see storm track labeled J4–J6 in Fig. 4a) approached Wisconsin; lower-tropospheric ascent (Fig. 11), moisture convergence, and moisture advection (Fig. 12) all acted to deepen the moist layer during this period. On 8 January, a well-developed cyclone (see storm track labeled J4–J15 in Fig. 4a; cyclonic flow in Fig. 14d) approached

Unauthenticated | Downloaded 05/10/21 09:57 PM UTC

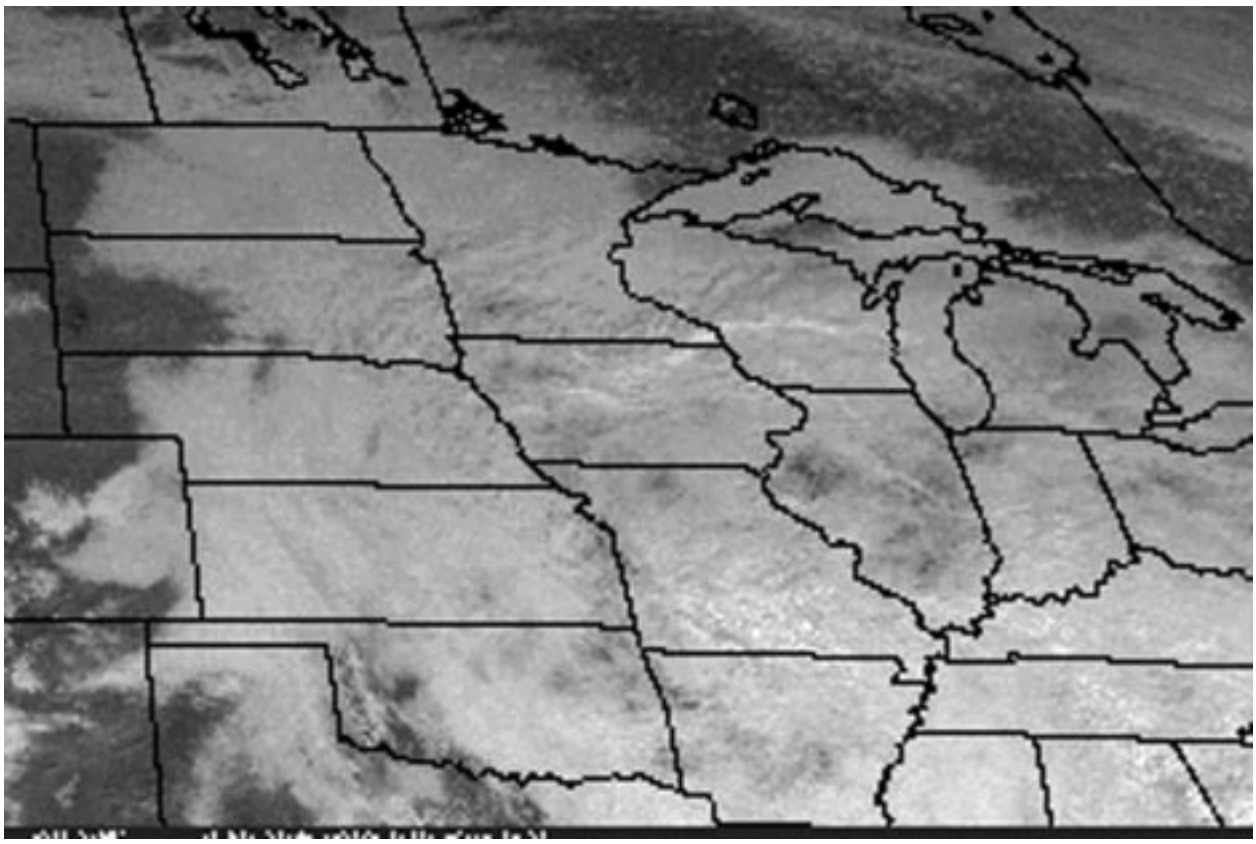

FIG. 13. *GOES-7* 2-km resolution visible imagery for 1801 UTC 28 December 1991.

Wisconsin. In advance of it, the lower-tropospheric moisture was deepened still further (Fig. 11) through strong moisture convergence and moist advection (Fig. 12), with 9.9 mm of precipitation reported at MKE. However, the sharp cold advection (Fig. 8) in the wake of its passage on 9–10 January led to strong tropospheric descent (Fig. 11), moisture divergence, and dry air advection (Figs. 12 and 14d), and signaled the end of the PLOE after 15 nearly continuous days of low cloud. PBL model simulations with implied temperature advections included showed enhanced lifting of the cloud layer, suggesting that the cold advection was a contributing factor to the breakup.

As a means of testing the sensitivity of this case to the strength of the solar radiation, simulations with the solar declination set to that of the first day of summer were also run (curves labeled SUM in Figs. 10a and 10b). Except for those days in which significant tropospheric ascent was occurring in response to mobile synoptic-scale systems (e.g., 2 January, 7–8 January), the low overcast failed to develop. For example, on 28 December (the onset period during which the inversion develops under subsidence), the summer solar radiation produces warming and drying of the surface layer (~6°C and ~35% relative humidity), the inversion erodes, and the cloud dissipates. Similarly, on 5 January, when the inversion has become reestablished following the passage of the 2 January cyclone, erosion of the inversion and dissipation of the cloud occurs with summer radiation (with warming–drying of ~5°C and ~25% relative humidity).

As noted above, an option exists in the model to turn off infrared radiative transfer. This option was exercised in a sensitivity test to determine the importance of infrared radiation from the top of the cloud layer in the growth and maintenance of the PLOE phenomenon (curves labeled NIR in Figs. 10a and 10b). The results indicate an infrared cooling rate of approximately 1°C occurs within and below the cloud layer, leading to an additional moistening of 2%–5%. During much of the PLOE, the loss of this cooling was sufficient to fully dissipate the cloud. Stratification of the simulations for daytime and overnight periods showed similar effects at both times, suggesting that diurnal effects were of little importance. This conclusion is also supported by analyses of the GRB soundings at 0000 and 1200 UTC, which showed a limited diurnal signal in the thickness of the cloud layer.

In summary, the onset of the low overcast conditions in this case appears to be tied to synoptic-scale transport of low-level moisture, which once in place, is not significantly disrupted by subsequent weakly developed

Unauthenticated | Downloaded 05/10/21 09:57 PM UTC

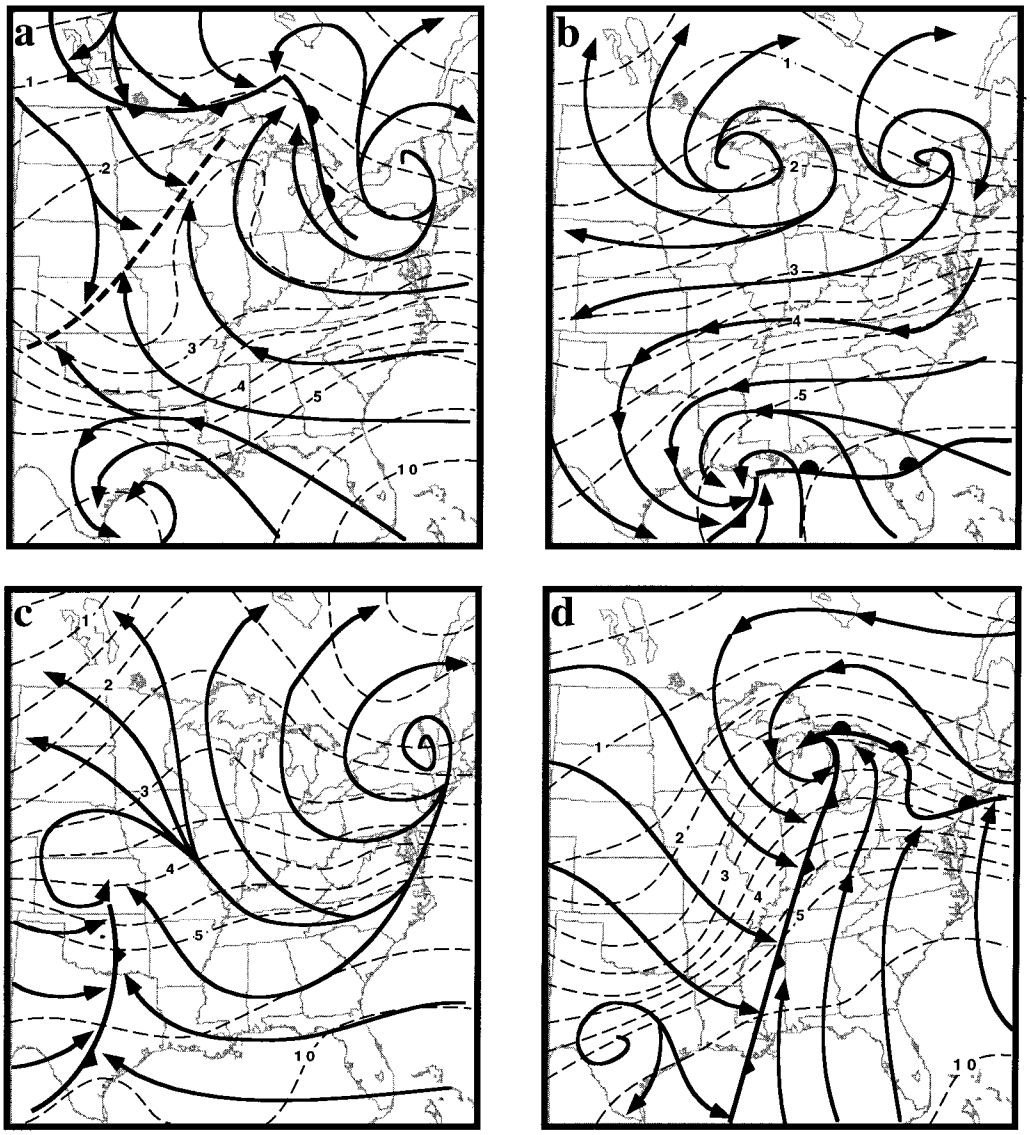

FIG. 14. The 950-hPa streamlines and surface to 900 hPa precipitable water (contours are every 0.5 mm to 5 mm, then every 2.5 mm) as obtained from sounding data. Also shown are surface fronts (standard symbols) and trough lines (thick dashed line). Map times are (a) 1200 UTC 26 December 1991, (b) 0000 UTC 28 December 1991, (c) 0000 UTC 2 January 1992, and (d) 1200 UTC 9 January 1992.

systems. Augmentation of the low-level moisture is periodically provided by moisture transport associated with these weak systems such that the subsidence following their passage is no longer capable of eroding the low cloud layer given the weak solar radiative input. Since Ekman pumping in the case of weak cyclones would tend to be maximized near the top of the PBL (e.g., Holton 1992, 133–138), it is plausible that such dynamics may have also played a role during the periods in which such cyclones were passing. Further enhancement can be provided by the evaporation of available surface moisture, although this source is not required. Breakup finally ensues following the passage of a well-developed baroclinic wave; in this case, drying of the moist layer through divergence of water vapor combined with horizontal transport of moisture out of the region is furthered by strong subsidence as surface high pressure builds in. The notable persistence of the cloud cover is due to the combination of the weak subsidence and weak solar input; an increase in either one of these factors is sufficient to dissipate the cloud.

4. Concluding discussion

This study has suggested that PLOEs in the upper Midwest, which on average occur slightly more often than once every two years, are promoted by the interaction of several subtle factors. Study of the circulation

Unauthenticated | Downloaded 05/10/21 09:57 PM UTC

signatures coincident with these events reveals that their occurrence is often tied to a split in the large-scale westerly jet, with downstream confluence of the northwesterly polar and the southwesterly subtropical jet streams. This flow results in a generally anticyclonic surface pressure pattern becoming established over the upper Midwest, occasionally disrupted by the emergence from either stream of relatively weak synoptic-scale weather systems. These systems act to moisten the affected region at low levels through horizontal transport of moisture and, to a lesser extent, moisture convergence. Subsidence inversions established following the passage of these systems act to erode the depth of the moist layer, but solar radiative input is insufficient during these cold season events to dissipate the cloud. Factors such as the (local) evaporation of surface moisture and the diurnal radiational cycle appear to be of secondary importance, since, although they contribute to the thickness of the cloud layer, such clouds would persist even without these contributions. The eventual end of the PLOE is induced by the passage of a well-developed baroclinic wave, whose dynamic attributes (dry air advection, moisture divergence) are sufficient to allow the strong subsidence that follows in its wake to fully dissipate the cloud.

However, it is important to note that other scenarios do occur. The 1972 PLOE featured a strong westerly jet stream and correspondingly frequent encounters with synoptic-scale systems (four in approximately 7 days). These systems were again relatively poorly developed and, thus, served to augment the low-level moisture in their advance, yet were incapable of eroding the cloud layers in the relatively unfavorable conditions (for cloud) in their wake. As might be suspected given the difficult balance that such a scenario entails, these conditions represent a minority of the PLOE events documented in the 30 yr of record studied here (see Table 2). Despite these differences, a common feature of the three cases examined in detail was reduced (composite) westerly airflow at or near the cloud layer (the 850-hPa level). This feature serves to emphasize the importance of self-sustaining mechanisms within the cloud layer, the primary agent of which, based upon experiments with a PBL model, appears to be infrared radiation from the top of the cloud layer.

The case study of the extremely long-lived PLOE of December 1991–January 1992 provides some insight into how forecasters might more confidently anticipate the onset and breakup of such events. Low-level moisture that is put in place primarily through the action of weak synoptic-scale cyclones (but that could conceivably be established through other means, including regional surface evaporation) is sufficient to begin such a period and should be easily recognizable. The critical and more difficult issue is whether or not the circumstances that allow the moisture to persist are also forecastable. These circumstances require that once the low cloud is established, it not be disrupted by strong dynamics (horizontal moisture flux divergence, cold air advection, and subsidence) or thermodynamics (moderate-to-strong solar radiative input). The properties of the event structure, from the large scale down to that of the cloud layer itself, are stable. For example, a PBL model simulation with initial time set to 1200 UTC 31 December 1991 (toward the end of the first extended period of subsidence following the passage of a weak cyclonic system) was run through several diurnal cycles with no indication of imminent breakup of the low cloud deck. Since the erosion of the cloud deck was minimal (see Figs. 8 and 11), augmentation of the moisture by weak cyclonic systems did not appear to be necessary to the continuance of this event (although such augmentation did periodically occur; see Figs. 11–12 and 14). Instead, the split flow pattern noted above reduces regional encounters with mobile weather systems and may facilitate such events by simply lowering the probability of encountering a disruptive system. The forecast difficulty is in assessing whether the forcing from such encounters, when they do occur, will be sufficient in a given case to terminate an established event. It is notable that although lifting of the cloud base began during the strong dynamics of 9 January (Figs. 8, 11, and 12), the end of the event was nonetheless delayed for an additional day.

Evidence of the difficulty of the forecast task is also provided in Table 3, which shows that in many cases split flow patterns *cannot* support the persistence of the low overcast. Despite the relative similarity of the large-scale flow, these episodes were of highly variable duration. For example, in the 10 September 1967 case, the storm track (tied to the position of the subtropical jet) was shifted slightly southward in comparison to 1991–92 such that the moisture input and dynamics were not present to initiate an event. On 2 November 1983, an inverted trough with weak 500-hPa support initiated low overcast at MKE, but it persisted for only 27 h. The soundings at GRB revealed deep moisture (up to 600 hPa) with precipitable water of 25 mm on that day. As strong surface high pressure built into the region on 3 November, a subsidence inversion developed and the deep moisture was removed (precipitable water dropped to 7 mm) with the remainder trapped below 900 hPa. However, unlike in 1991–92, surface winds at MKE were from the northeast at 10 m s^{-1}, promoting mixing, and peak solar radiative input to the atmosphere was relatively strong (approximately 30% higher). Consequently, on the morning of 3 November, the ceiling lifted and breaks in the overcast developed, ending the episode.

These episodes remain an operational forecast problem, despite the sophisticated guidance from the current generation of numerical weather prediction models. This statement is best addressed by reference to an event that occurred while revisions to this paper were in progress. Figure 15 shows a time series of observed and forecast (Nested Grid Model Output Statistics or NGM-MOS)

Unauthenticated | Downloaded 05/10/21 09:57 PM UTC

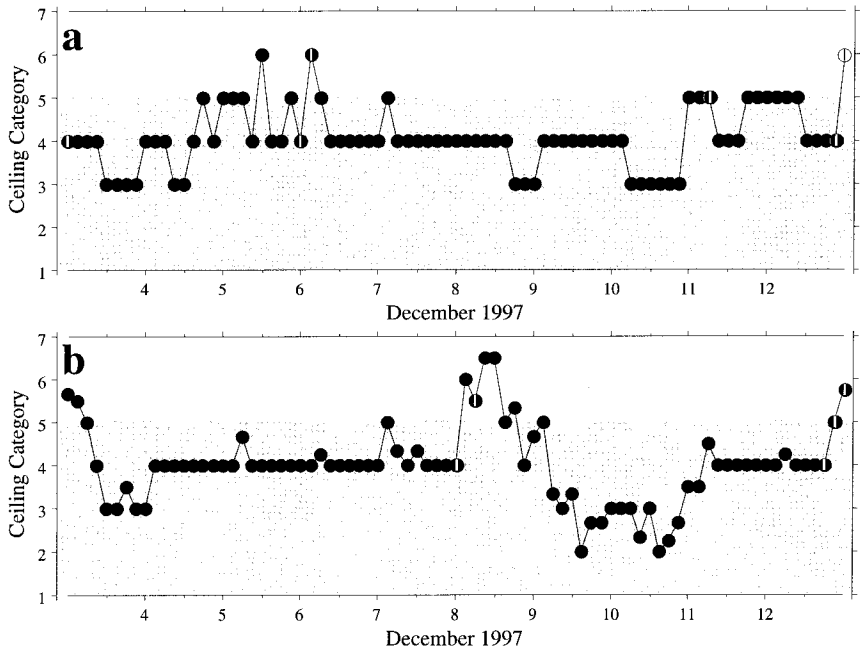

FIG. 15. Ceiling category and opaque cloud cover at ORD for 3–13 December 1997 from (a) observations and (b) NGM-MOS forecasts. The NGM-MOS forecasts are averaged over all available forecast ranges (6–48 h) for a given verification time. The observed and forecast ceiling categories are defined according to the NGM-MOS scale, where 1 is less than 61 m (200 ft), 2 is 61–122 m (200–400 ft), 3 is 152–274 m (500–900 ft), 4 is 305–914 m (1000–3000 ft), 5 is 945–1981 m (3100–6500 ft), 6 is 2012–4023 m (6600–12 000 ft), and 7 is greater than 4023 m (12 000 ft). The gray shading denotes the low cloud layer.

cloud ceiling and cloud cover at O'Hare International Airport (ORD) in Chicago. An extended period of cloudiness occurred at ORD from 3 to 12 December 1997, with occasional short breaks or lifting of the cloud base above 2 km (5–6 and 11 December; Fig. 15a). The NGM-MOS generally performed well in indicating an extended period of low cloud conditions through this time, and correctly forecast the end of the low cloud that occurred late on 12 December (Fig. 15b). Despite this, it was late in initiating the low overcast on 3 December, missed the short periods of cloud-base lifting and breaks on 5–6 and 11 December, and falsely forecast such lifting and breaks on 8 December. The period was marked by a split flow pattern at 500 hPa with weak flow at 850 hPa over the Great Lakes region, consistent with the dominant flow configuration associated with PLOEs in the Midwest.

Given these results, it is clear that synoptic-scale signatures obtainable from the current generation of forecast models would not alone be sufficient to provide a confident forecast regarding the evolution of the low cloud during an event, except under extreme circumstances (i.e., intense subsidence). However, the use of standard forecast model guidance (MOS and forecast vertical motions) in conjunction with boundary layer modeling would provide a means to test the uncertainty of a given forecast. Relatively simple models such as the one employed here could be used in a real-time ensemble mode to establish the likelihood of event termination, given certain ranges of error in the forecast guidance. As an example, we have conducted some experiments with the PBL model for 8 December 1997, a time when the cloud conditions at ORD were relatively poorly forecast by the NGM-MOS. The NGM predicted 700-hPa subsidence in the range of 0–2 cm s^{-1} on 8 December, with the later forecasts tending toward weaker sinking. The PBL model experiments (initialized using the 1200 UTC 7 December sounding at Davenport) revealed the full range of possibilities: subsidence as high as 2 cm s^{-1} would eliminate the cloud deck entirely while weaker sinking would produce little or no lifting of and breaks in the low overcast (as was observed). Although reasonable treatments of the PBL are already incorporated into existing operational models, the sensitive dependence of its evolution on complex interactions between variables allows little opportunity for forecasters to assess the limitations of the guidance and fine-tune their forecasts accordingly. Such a capability would clearly be of value both to forecasters and to the end users of those forecasts.

Acknowledgments. Special thanks are directed to Dr. Brad Colman of the Seattle Weather Service Forecast Office (WSFO) for supplying us with the Blackadar PBL model code. We also thank Bob McMahon of the Sioux Falls WSFO for supplying MSN hourly observations

Unauthenticated | Downloaded 05/10/21 09:57 PM UTC

and Paul Dallavalle of NOAA-TDL for regenerating the NGM-MOS forecasts for the 1991–92 case. Finally, we thank Da-Lin Zhang and the two anonymous reviewers for their many helpful suggestions that strengthened our presentation of this work.

REFERENCES

Arya, S. P., 1988: *Introduction to Micrometeorology*. Academic Press, 303 pp.

Bellamy, J. C., 1949: Objective calculations of divergence, vertical velocity and vorticity. *Bull. Amer. Meteor. Soc.*, **30,** 45–49.

Blackadar, A. K., 1976: Modeling the nocturnal boundary layer. Preprints, *Third Symp. on Atmospheric Turbulence and Air Quality*, Raleigh, NC, Amer. Meteor. Soc., 46–49.

——, 1979: High resolution models of the planetary boundary layer. *Advances in Environmental Science and Engineering*, J. R. Pfaffin and E. N. Ziegler, Eds., Gordon and Breach, 50–85.

——, 1997: *Turbulence and Diffusion in the Atmosphere: Lectures in Environmental Sciences*. Springer-Verlag, 185 pp.

Bosart, L. F., and F. Sanders, 1981: The Johnstown flood of July 1977: A long-lived convective system. *J. Atmos. Sci.*, **38,** 1616–1642.

Carlson, T. N., and F. E. Boland, 1978: Analysis of urban-rural canopy using a surface heat flux/temperature model. *J. Appl. Meteor.*, **17,** 998–1013.

Deardorff, J. W., 1978: Efficient prediction of ground surface temperature and moisture with inclusion of a layer of vegetation. *J. Geophys. Res.*, **83,** 1889–1904.

Dimego, G. J., K. E. Mitchell, R. A. Petersen, J. E. Hoke, J. P. Gerrity, J. T. Tuccillo, R. L. Wobus, and H.-M. H. Juang, 1992: Changes to NMC's regional analysis and forecast system. *Wea. Forecasting*, **7,** 185–198.

Epstein, E. S., 1969: A scoring system for probability forecasts of ranked categories. *J. Appl. Meteor.*, **8,** 985–987.

Hollingsworth, A., K. Arpe, M. Capaldo, and H. Savijari, 1980: The performance of a medium range forecast model in winter—Impact of physical parameterizations. *Mon. Wea. Rev.*, **108,** 1736–1773.

Holton, J. R., 1992: *An Introduction to Dynamic Meteorology*. Academic Press, 511 pp.

Lorenz, E., 1969: Atmospheric predictability as revealed by naturally occurring analogues. *J. Atmos. Sci.*, **26,** 636–646.

Mass, C. F., H. J. Edmon, H. J. Freidman, N. R. Cherney, and E. E. Recker, 1987: The use of compact discs for storage of large meteorological and oceanographic data sets. *Bull. Amer. Meteor. Soc.*, **68,** 1556–1558.

Morgan, M. D., and J. M. Moran, 1997: *Weather and People*. Prentice-Hall, 200 pp.

O'Brien, J. J., 1970: Alternative solution to the classical vertical velocity problem. *J. Appl. Meteor.*, **9,** 197–203.

Oke, T. R., 1978: *Boundary Layer Climates*. John Wiley and Sons, 372 pp.

Oncley, S. P., and J. Dudhia, 1995: Evaluation of surface fluxes from MM5 using observations. *Mon. Wea. Rev.*, **123,** 3344–3357.

Roebber, P. J., and L. F. Bosart, 1998: The sensitivity of precipitation to circulation details. Part I: An analysis of regional analogs. *Mon. Wea. Rev.*, **126,** 437–455.

Schultz, G., 1986: *Wisconsin's Foundations. A Review of the State's Geology and Its Influence on Geography and Human Activity*. Kendall-Hunt Publishing, 211 pp.

Sellers, W. D., 1965: *Physical Climatology*. University of Chicago Press, 272 pp.

Shea, B., 1996: Study of low cloud formation and duration at Little Rock, Arkansas. NOAA Tech. Memo. NWS SR-180, 12 pp. [Available from National Technical Information Service, 5285 Port Royal Road, Springfield, VA 22161.]

Shuman, F. G., and J. B. Hovermale, 1968: An operational six-layer primitive equation model. *J. Appl. Meteor.*, **7,** 525–547.

Twomey, S., 1991: Aerosols, clouds and radiation. *Atmos. Environ.*, **25A,** 2435–2442.

WMO, 1975: *Manual on the Observation of Clouds and Other Meteors*. Vol. I, *International Cloud Atlas*, World Meteorological Organization, 62 pp.

Zhang, D. L., and R. A. Anthes, 1982: A high-resolution model of the planetary boundary layer—Sensitivity tests and comparisons with SESAME-79 data. *J. Appl. Meteor.*, **21,** 1594–1609.

Unauthenticated | Downloaded 05/10/21 09:57 PM UTC